Grain boundary diffusion of Ag through polycrystalline SiC in TRISO fuel particles

Jie Deng[a], Hyunseok Ko[a], Paul Demkowicz[b], Dane Morgan[a,c], Izabela Szlufarska[a,c,*]

[a]*Department of Materials Science and Engineering, University of Wisconsin-Madison, Madison, WI 53706*
[b]*Idaho National Laboratory, P.O. Box 1625, Idaho Falls, ID 83414*
[c]*Department of Engineering Physics, University of Wisconsin-Madison, Madison, WI 53706*

Abstract

The effective diffusivity and release fraction of Ag in polycrystalline SiC are evaluated using a kinetic Monte Carlo model. The effects of various grain boundary network properties on the transport of Ag across the SiC layer have been examined, including fraction of grain boundary type, spread in grain boundary diffusivities and distribution of grain boundary types. It is shown that the effective diffusivity and release fraction of Ag can exhibit a large variability due to changes in the GB structure of SiC, and this variability is almost independent of temperature fluctuation. The present results suggest that the variation in properties of grain boundary networks in SiC may contribute to the spread in the Ag diffusivity and release fraction measured in TRISO particles. It is also found that the grain boundary diffusion alone may be insufficient to account for the Ag diffusivities and release fractions measured in integral release experiments. Additional factors such as irradiation and temperature distribution may also play an important role in Ag transport across the SiC layer.

Keywords: Grain boundary diffusion, TRISO fuel particles, Fission product release

1. Introduction

The tristructural-isotropic (TRISO) fuel particle is one of the main fuel forms used in the very high temperature reactors (VHTR) [1]. A fuel particle consists of a spherical fuel kernel surrounded by a porous graphite buffer layer and three coating layers [2, 3]: inner pyrolytic carbon layer, SiC layer, and outer pyrolytic carbon layer. Each coating layer has its own functionality, and one of the main functions of the SiC layer is to prevent the radioactive fission products from diffusing out into the coolant [4]. It has been observed in reactor experiments that although the SiC layer can retain most fission products, some species such as Ag can escape from fuel particles [5–10]. For example, Nabielek *et al.* [5] carried out in-pile experiments in the Dragon reactor and found that the content of Ag retained in individual fuel particles after irradiation has drastic variations. In addition Ag release was found to be significantly increased at fuel operating temperatures above 1200°C. Amian *et al.* [6] and Verfondern *et al.* [7] conducted post-irradiation annealing tests on coated particles at temperatures between 1000°C and 2100°C, where the coated particles had been irradiated in a wide range of temperature, burnup and fluence. It was found that Ag was released

*Corresponding author. Tel: +1 608-265-5878; Fax: +1 608-262-8353.
Email address: szlufarska@wisc.edu (Izabela Szlufarska)

in all cases considered, and that there was a large scatter in the Ag diffusivity in individual fuel particles. Bullock *et al.* [8] carried out post-irradiation annealing tests on different types of TRISO fuel particles at three different temperatures (1200°C, 1350°C and 1500°C). It was shown that for SiC coated particles, Ag was released at 1500°C only and, as in the earlier experiments, Ag release varied strongly from particle to particle. Recently Demkowicz *et al.* [9] and Baldwin *et al.* [10] presented results of post-irradiation examination of the Advanced Gas Reactor (AGR) TRISO fuel compacts that experienced a wide range of irradiation temperatures and a significant spatial variation in temperature within a single compact. It was shown that the fractional release of Ag from particles can be quite significant. Individual compacts within a single capsule exhibited significantly different Ag retention, and within a single compact individual particles exhibited a wide range of Ag release. These experimental results suggest that the release of Ag can be significant in TRISO fuel elements at high temperatures (above approximately 1000°C-1100°C) and moreover, that there is a high variability in the release fraction and diffusivity of Ag in individual fuel particles. The release of Ag from fuel has safety implications related to plant maintenance, as it can deposit on surfaces in the helium coolant circuit. In order to better design the TRISO fuel particles, it is critical to understand transport mechanisms of Ag across the SiC layer and to identify the causes of variability in the degree of Ag release.

The mechanisms of Ag moving across the SiC layer are still under debate [11–24]. One proposed mechanism is that Ag escapes from fuel particles via vapor diffusion along cracks in the SiC layer [12, 13]. This argument was presented for example by MacLean *et al.* who investigated transport of Ag implanted into polycrystalline β-SiC [12, 13]. As the authors did not observe any Ag diffusion through SiC in their experiments, they concluded that in reactor conditions Ag may diffuse along cracks in SiC. These cracks could be generated during fabrication or irradiation exposure. The mechanism of diffusion along cracks is consistent with results of *ab initio* calculations based on the density functional theory (DFT) [14], which showed that Ag prefers to absorb on the SiC surface rather than remain in the bulk and that the mobility of Ag on the SiC surface is high. However, there might be other reasons why Ag did not diffuse in the experiments reported in Refs. [12, 13] and yet be possible in reactor conditions. For instance, in the laboratory experiments implantation introduced a highly amorphous layer in SiC and it is possible that this amorphization led to Ag being trapped in precipitates. An amorphous implantation layer is unlikely to occur under reactor conditions. In addition, recent experiments by Minato *et al.* [15] and Lopez-Honorato *et al.* [16] showed that the release behavior of Ag cannot be explained only by the presence or absence of the cracks in the SiC layer because some particles with no cracks in the SiC have very poor Ag retention. The above findings indicate that although the presence of cracks could accelerate Ag transport, cracks are not the only transport pathway, and perhaps not even the dominant one. Another proposed mechanism for fast Ag release is the chemical degradation of SiC by fission products such as Pd [17–19]. Neethling *et al.* [17–19] showed that Pd can react with SiC and form palladium silicides along grain boundaries (GBs) of SiC. These palladium silicides can interact with Ag and form a Pd, Ag, and Si solution that is capable of migrating along GBs in SiC over time. These results suggest that the presence of Pd may facilitate the migration of Ag in SiC. On the other hand, Minato *et al.* [20] found high Ag release in fuel particles where Pd attack was not observable using optical microscopy, which may indicate that Ag can transport in SiC without assistance of Pd.

In addition to vapor diffusion and chemical degradation, GB diffusion is another potential mechanism for Ag transport in SiC [16, 21–24]. Friedland *et al.* [21, 22] implanted Ag in SiC and

compared migration of Ag in single crystal SiC and polycrystalline SiC at 1300°C. Ag diffusion was observed to take place in the latter but not the former structure, which implies that Ag can be transported in SiC via GB diffusion. In addition, Lopez-Honorato *et al.* [16, 23] developed a method of trapping thin layers of Ag between two SiC layers in actual coated fuel particles. In their experiments, Ag was clearly detected at GBs, which shows that migration of Ag is at least partially governed by GB diffusion. Recently, Gerczak *et al.* [24] compared the transport of Ag implanted into single crystal 4H-SiC and polycrystalline chemical-vapor-deposited 3C-SiC at 1500°C, 1535°C, 1569°C and 1625°C. The penetration of Ag into the bulk past the primary implantation peak is not observed in 4H-SiC, but is found in 3C-SiC after thermal exposure above 1535°C. These results imply that the presence of GBs may facilitate Ag diffusion above 1535°C. In addition to the experimental investigations, DFT calculations demonstrated that in SiC the diffusivity of Ag along GBs [25–27] is much higher than that in bulk [28], which suggests that GBs in SiC may provide fast-diffusion paths for Ag migration. Moreover, microstructures of SiC in TRISO fuel particles have been examined by electron back scatter diffraction [29–31], where it was shown that GB characters in SiC can vary significantly among different particles. Since the diffusivity of Ag in GBs presumably depends on the characters of GBs, it is expected that different distributions of GB character may lead to fluctuation in the overall transport of Ag across the SiC layer. Therefore, these previous studies suggest that GB diffusion may not only account for fast Ag transport in SiC, but also be responsible for at lease some of the variability in diffusivity and release fraction of Ag measured in integral release experiments shown in Refs. [5–10].

The present study focuses on GB diffusion of Ag in the SiC layer and aims to test two hypotheses: (i) the variation in GB structures may be the origin of some or all of the scatter in diffusivity and release fraction of Ag in TRISO fuel particles; (ii) GB diffusion in polycrystalline SiC is fast enough to explain experimentally observed Ag release. To test these hypotheses, we use our recently developed kinetic Monte Carlo (kMC) model [32] for diffusion through polycrystalline materials and calculate the effective diffusivity of Ag in heterogeneous GB networks in SiC. The model is also further extended to evaluate the release fraction of Ag in fuel particles with time-dependent generation of Ag. We demonstrate the dependence of the effective diffusivity and release fraction of Ag on various properties of GB networks such as GB distribution and fraction of each GB type. We also examine the role of GB structure and temperature variation in the fluctuation of Ag transport and discuss additional factors that may affect GB diffusion of Ag in actual fuel particles, such as irradiation damage and temperature distribution.

2. Kinetic Monte Carlo Model

In our kMC model, the GB network of SiC is represented by a three-dimensional (3D) Voronoi diagram. In order to approximate the spherical shell structure of the SiC layer with a simpler geometry, the simulation domain is assumed to be a rectilinear block where the dimensions in the x and y directions (denoted by Lx and Ly, respectively) are much larger than that in the z direction (denoted by Lz), see Fig. 1 for a schematic diagram. Here x, y and z directions represent three orthogonal directions in a 3D space, where the x and y directions are parallel to the tangent of the coating surface, and the z direction is normal to the coating surface. In a typical fuel particle, the SiC layer has a thickness of 35 μm with the inner surface area around $1 - 2$ mm^2. Thus the simulation domain is set to be Lz = 35 μm and Lx = Ly = 32 Lz. In an ideal simulation we would generate a Voronoi diagram directly in this domain, and then mesh each GB plane by triangular elements so that a Ag atom can hop along an element edge (from one mesh node to another

neighboring node) along GBs. However, considering the typical grain size (0.5 μm - 2.5 μm) in a SiC layer, the number of GBs in the simulation domain is more than 10^7 and meshing all of them is not numerically practical. Therefore, to simplify the numerical problem in this study, we assume that the simulation domain consists of $32 \times 32 = 1024$ connected cubic boxes, each with the edge size equal to Lz. We first generate a Voronoi diagram in one box and mesh each GB within this box using triangular elements. Subsequently we assume that the same Voronoi diagram represents well the GB topology in each of the 1024 boxes, and simply replicate the Voronoi diagram across all of the boxes. Having assigned the Voronoi diagram in all boxes, we then assign a random diffusivity to each GB in the entire simulation domain. In other words, each of the 1024 boxes share the same Voronoi diagram but have different distributions of GB diffusivities. In order to test how a specific assignment of the Voronoi diagram influences the effective diffusivity in a single box, we calculated the effective diffusivity (see below for method of calculation) in a cubic box of size Lz with different Voronoi diagrams. In all these test simulations we kept the average grain size constant. We found that the magnitude and distribution of the effective diffusivity is almost independent of the Voronoi diagram used in the box, with variations in effective diffusivity among different Voronoi diagrams being lower than 5%. Thus from the perspective of our diffusion study, the procedure of using a single Voronoi diagram for all the boxes is an excellent approximation of the more realistic case where GB topology varies among the boxes.

With the GB networks of SiC built as described above, the effective diffusivity of Ag moving across such networks is calculated as follows. A Ag atom is placed at a randomly selected mesh node at the beginning of the simulation, and then it diffuses in the domain via hops along element edges. In each kMC step, the Ag atom randomly chooses to move along an element edge i based on the rate $\Gamma_i = \frac{D_i}{l_i}$, where D_i and l_i are the diffusivity and length of the element edge i, respectively. After each kMC step, the total diffusion time t and the total displacement d_z along the z direction are recorded. Displacement d_z is calculated as a projection on the z direction of the distance between the current and the initial positions of the Ag atom. Periodic boundary conditions are applied in all spatial directions. After a sufficiently long time (long enough to obtain converged results), the effective diffusivity can be calculated as $D_{\text{eff}} = \frac{d_z^2}{2t}$. Note that this is technically the effective diffusivity along just the z direction. Given that diffusion along the z direction is the relevant parameter for Ag release we take this as the effective diffusivity in this work. In addition, the effective diffusivity is largely isotropic, with very minor anisotropy emerging from the modeling approach, and the z diffusivity is therefore very close to the full isotropic effective diffusion coefficient. We repeat this procedure for 10^4 samples (each sample has 1024 boxes, and they share the same Voronoi diagram but have different GB distributions) and then we obtain the average effective diffusivity $\langle D_{\text{eff}} \rangle$ of Ag through polycrystalline SiC. A more detailed description of our model can be found in Ref. [32].

The model described above can be applied both to the case where temperature is constant and where it changes as a function of time. The model can also be extended to evaluate the release fraction of Ag when the generation rate of Ag is time-dependent. When calculating the release fraction of Ag, periodic boundary conditions are applied along x and y directions only. We further denote the z- and z+ planes (two boundary planes in the z direction) as the inner and outer surface of the SiC layer, respectively. The diffusivity of a Ag atom along the SiC surface or in the inner region of a fuel particle (e.g., the porous buffer layer) is generally larger than the GB diffusivity in SiC. In order to capture the fast transport of Ag on the inner surface of SiC (or within the inner buffer layer), we add a virtual node and place it outside the SiC layer. The virtual node is connected to each node in the z- plane by virtual paths so that a Ag atom can diffuse back

and forth between any node on the z- plane through the virtual node see Fig. 1 for a simplified illustration. The Ag diffusivity along each virtual path is assumed to be the same and much larger than the GB diffusivity of Ag in the SiC layer, thus effectively connecting all the nodes on the z- plane with a fast diffusion path. In each simulation, a Ag atom starts at the virtual node, and the atom is assumed to be released if it can reach the z+ plane within its diffusion time. Let us assume that Ag is generated (with some known dependence of the generation rate on time) between time 0 and time τ, where τ represents the total time of an in-pile experiment for a fuel. The release fraction of Ag at time τ can be calculated as follows. We first divide τ into m intervals, i.e., the first interval $[t_0, t_1]$, the second interval $[t_1, t_2]$, ..., the m-th interval $[t_{m-1}, t_m]$, where $t_0 = 0$, $t_m = \tau$ and $t_i - t_{i-1} = \tau/m$ for $i = 1, ..., m$. Denote n_i as the number of Ag atoms generated in the i-th interval $[t_{i-1}, t_i]$. For the sake of numerical efficiency, we assume that n_i Ag atoms are generated at a specific time, which we take as $\langle t_i \rangle = (t_i + t_{i-1})/2$. Then the release fraction of Ag at τ can be expressed as $F = \sum_{i=1}^{m}(f_i n_i)/\sum_{i=1}^{m} n_i$, where f_i is the release fraction of the Ag atoms generated at the i-th interval. f_i represents the probability of moving more than the thickness of the SiC layer in the z direction (i.e., reaching the z+ plane) during the diffusion time $\tau - \langle t_i \rangle$.

We note that there are several assumptions in our model. First, the only active transport mechanism of Ag in the model is GB diffusion. Bulk diffusion is not considered because Ag has a strong tendency to segregate to SiC GBs and the GB diffusivity of Ag is much higher than its bulk diffusivity [25, 26, 28]. Secondly, the hop of Ag atoms is coarse-grained (from one mesh node to another) rather than atomic. However, it has been demonstrated in Ref. [32] that with the appropriate hopping rate, the kMC model with coarse-grained hops yields the same effective diffusivity as a model with atomic resolution. Thirdly, the difference between the diffusion of Ag along GB junctions and within GB planes is ignored here. While diffusion along the GB junction is generally different from diffusion within GB planes, their difference depends on temperature and GB structure, and there is currently no quantitative data for Ag diffusivity along GB junctions of SiC that would allow us to include this distinction in our model. As such, in the current model the diffusion coefficient for transport along a GB junction is set to be the highest diffusion coefficient in all GBs that connect to that GB junction. The most significant approximation in the model is likely the use of just two GB diffusivities whose values are adapted as best as possible from modeling and experimental results, as described in Sec. 3. This approximation is necessitated by the fact that the Ag diffusion coefficients are not known for general GB types.

We note that kMC models have been previously applied by other researchers to examine transport of Ag across the three coating layers in TRISO fuel particles [34]. The model developed in Ref. [34] assumes that Ag has a single diffusivity in each coating layer and each layer consists of rectangular grains. The influence of a number of microstructural features (such as reflective interfaces, cracks and radiation-induced cavities) on Ag transport were taken into account using parametric functions that may either accelerate or retard Ag diffusion. The results showed that it is possible to fit integral release experimental data by varying parameters in the model. In contrast to this earlier study, in our model we focus on GB diffusion in the SiC layer and we consider a 3D GB network with properties similar to those measured in experimental SiC samples. No other types of defects or microstructural features are included, which isolates other influences on Ag diffusion and allows us to test whether GB diffusion alone may account for fast Ag diffusion in SiC as well as the variability in Ag release behavior.

3. Grain boundary diffusion of Ag in SiC

The kMC model introduced in Section 2 is applied to evaluate the effective diffusivity and release fraction of Ag in polycrystalline SiC. In order to provide insights into Ag transport in fuel particles, the properties of GB networks in the SiC layer in actual TRISO fuel particles shown in Refs. [29, 35] are used in our model. Specifically, the simulation domain is a rectilinear block, where the surface area is similar to the area of the inner surface of the SiC coating in TRISO and the domain thickness is 35 μm, which is a typical thickness of the SiC layer. The domain contains about 4.1×10^6 grains and the average grain size is 2.2 μm, which is within the range of typical grain size (0.5 μm - 2.5 μm) found in TRISO particles. The GB character in the SiC layer has a wide distribution, which includes various coincidence site lattice (CSL) GBs, low- and high-angle GBs. Although a few simulation studies reported diffusion coefficients along specific GBs in SiC [25–27], a general dependence of Ag diffusion coefficient on GB type is still unknown. As such, in our model we assume that two types of GBs, low-energy GB (LEGB) and high-energy GB (HEGB), are randomly distributed throughout the sample. The diffusivities of Ag along LEGB and HEGB, denoted by D_{L} and D_{H}, respectively, represent the lower and upper limit of Ag diffusion along GBs in SiC.

The range of the fraction of LEGB, f_{L}, is determined as follows. The electron backscatter diffraction measurement on AGR-1 fuel particles shows that the range of the fraction of CSL GBs, low-angle GBs and high-angle GBs in the SiC layer is 0.3 - 0.45, 0.1 - 0.15, and 0.4 - 0.6, respectively [35]. We assume that these values are at least approximately representative of other TRISO particle SiC grown by chemical vapor deposition in previous integral release experiments. In the case when only CSL GBs can be counted as LEGBs (a lower bound for LEGB fraction), the minimum f_{L} is 0.3. In the case when only high-angle GBs can be counted as HEGBs (an upper bound for LEGB fraction), the maximum f_{L} is 0.6. Therefore, the range of f_{L} can be approximated as 0.3 - 0.6. Correspondingly, the fraction of HEGB, f_{H}, varies from 0.4 to 0.7 in our model.

The values of D_{L} and D_{H} in the present study are assumed to be $D_{\mathrm{L}} = 10^{-9} \times \exp\left(\frac{-2.7}{kT}\right)$ m^2/s, and $D_{\mathrm{H}} = 10^{-9} \times \exp\left(\frac{-2.04}{kT}\right)$ m^2/s. These values are chosen to meet the following constraints and assumptions:

1. The values are such that in the relevant temperature range 900°C - 1400°C, the diffusivity ratio $\frac{D_{\mathrm{H}}}{D_{\mathrm{L}}}$ varies from 10^2 to 10^3, which is reasonable for impurity diffusion in polycrystalline materials [36].
2. The variation in values are due to activation energies, rather than attempt frequencies, as the latter are not expected to vary dramatically with GB type. The attempt frequencies are set to values from fitted D values for integral release in Refs. [5–7].
3. The activation energies should be close to 2.2 eV, which is approximately the value observed in integral release experiments [5–7].
4. The specific values of the activation energies for D_{L} and D_{H} are then selected to ensure that when f_{H} varies from 0.4 and 0.7, the effective diffusivities of Ag are between the lower and upper limits of the Ag diffusivity measured in Refs. [5–7]. This approach assures that our overall predicted D values are consistent with the average integral release experiments. It also allows us to assess the variation in diffusivity with variation of the specific spatial distributions of GB types for fixed f_{H}, which is the focus of Sections 3.1 and 3.2.

It is emphasized here that although the diffusivity ratio in our model can be as large as 10^2 or 10^3, it does not mean that the effective diffusivity D_{eff} will vary 2 or 3 orders of magnitude. The

actual fluctuation of D_{eff}, which is one of the main interests of this study, remains to be examined because D_{eff} is not only dependent on D_{L} and D_{H}, but it is also affected by f_{H}, as well as by the connectivity of GBs [32, 37]. We note that by fitting the values of diffusivities to release data from Refs. [5–7] we can assess our first hypothesis, that GB structure may be a significant source of variation in integral release values, but we cannot assess our second hypothesis, that Ag integral release can be explained by GB diffusion, as our release will be reasonably consistent with experiments by construction. These fitted diffusivity values will therefore only be used to assess the first hypothesis, as done in in Sec. 3.1-3.3. The second hypothesis will be tested in Sec. 3.4 using GB diffusivities estimated from published quantitative data distinct from integral release based estimates.

3.1. Effect of GB network properties on the effective diffusivity at constant temperature

With the GB diffusivities of Ag and properties of GB networks in SiC shown above, we first examine the effective diffusivity of Ag at a constant temperature. Because temperature is constant throughout the simulation time, the diffusivities D_{L} and D_{H} are independent of time as well. In the following figures, $\langle D_{\text{eff}} \rangle$ is normalized by D_{L} so that the features of $\langle D_{\text{eff}} \rangle$ are not affected by the diffusivity unit. Normalization of $\langle D_{\text{eff}} \rangle$ does not alter its dependence on properties of GB networks.

Figure 2a shows $\frac{\langle D_{\text{eff}} \rangle}{D_{\text{L}}}$ as a function of f_{H} with different diffusivity ratios $\frac{D_{\text{H}}}{D_{\text{L}}}$. It can be seen that for larger values of $\frac{D_{\text{H}}}{D_{\text{L}}}$, $\langle D_{\text{eff}} \rangle$ increases more rapidly with f_{H}. The dependence of $\langle D_{\text{eff}} \rangle$ on $\frac{D_{\text{H}}}{D_{\text{L}}}$ for different values of f_{H} is shown in Fig. 2b. We find that in most cases D_{eff} is strongly dependent on $\frac{D_{\text{H}}}{D_{\text{L}}}$ and that this dependence is almost linear. Figures 2a and 2b show that the effective diffusivity of Ag may vary significantly as the properties of GB networks in SiC change. This result suggests that decreasing the variability in GB characters may reduce the scatter in Ag diffusivity.

As mentioned in Section 2, the effective diffusivities shown in Fig. 2 are averaged over 10^4 samples with different GB distributions. D_{eff} exhibits fluctuations among these samples because of the statistical nature of GB distributions. It is instructive to investigate the fluctuation of D_{eff} since it reveals the dependence of D_{eff} on the randomly sampled microstructure and gives an estimate of the range of D_{eff} values that can be measured in different samples with the same dimensions, with the same f_{H} and the same $\frac{D_{\text{H}}}{D_{\text{L}}}$. Here, we characterize the fluctuation of D_{eff} using the coefficient of variation, $c_v = \frac{\sigma}{\mu}$, where μ is the average effective diffusivity and σ is the standard deviation of D_{eff}. Figure 3a shows how c_v depends on the values of f_{H} and $\frac{D_{\text{H}}}{D_{\text{L}}}$. Two main conclusions can be drawn from this figure. First, c_v is almost independent of f_{H} and $\frac{D_{\text{H}}}{D_{\text{L}}}$, which indicates that macroscopic properties of GB networks such as f_{H} and $\frac{D_{\text{H}}}{D_{\text{L}}}$ have a minor effect on the fluctuation of D_{eff} induced by microstructural changes. Secondly, in all cases c_v is larger than 1. It demonstrates that, with typical GB structures in SiC, the fluctuation of D_{eff} due to variation in GB distributions can be significant. The latter is confirmed in Fig. 3b, which gives typical distributions of $\frac{D_{\text{eff}}}{\langle D_{\text{eff}} \rangle}$ with different f_{H} and $\frac{D_{\text{H}}}{D_{\text{L}}}$. Since both D_{eff} and $\langle D_{\text{eff}} \rangle$ are affected by f_{H} and $\frac{D_{\text{H}}}{D_{\text{L}}}$, in order to compare the diffusivity probability distribution at different values of f_{H} and $\frac{D_{\text{H}}}{D_{\text{L}}}$, in Fig. 3b we plot it as a function of $\frac{D_{\text{eff}}}{\langle D_{\text{eff}} \rangle}$ instead of D_{eff}. It allows us to obtain a master curve for the probability

distribution of the diffusivity, which is almost independent of f_{H} and $\frac{D_{\mathrm{H}}}{D_{\mathrm{L}}}$. Fig. 3b shows that D_{eff} may vary one order of magnitude due to the change in GB distribution. Note that the scatter in the probability distribution for large values of $\frac{D_{\mathrm{eff}}}{\langle D_{\mathrm{eff}} \rangle}$ is statistical in nature. Figure 3 demonstrates that in addition to macroscopic properties of GB networks, distribution of GBs can also contribute to the scatter in Ag diffusivity measured in individual fuel particles.

3.2. Effect of GB network properties on the effective diffusivity with time-dependent temperature

The data in Figs. 2 and 3 were generated under conditions of constant temperature. In actual operating conditions of reactors, temperature fluctuates with time. Therefore, it is important to examine the dependence of the effective diffusivity of Ag on GB structures when temperature (and thus GB diffusivity) is time-dependent. In order to show the effect of temperature fluctuation clearly, we assume that temperature changes as a linear function of time, and the initial values are chosen so as to yield the same average temperature for all cases. Figure 4a shows temperature profiles for 5 different cases we studied, where the temperature change from time 0 to 600 days is 0°C, 60°C, 120°C, 180°C, and 240°C. The range of time-averaged, volume-averaged irradiation temperatures in AGR-1 fuel compacts is approximately 200°C [9], which is within the range of temperature variation considered here. The total simulation time (600 days) is also similar to the total operation time in the AGR-1 irradiation test [38].

In Fig. 4b we plot the dependence of the effective diffusivity on f_{H} with the different temperature profiles shown in Fig. 4a. It can be seen that both the temperature history and GB structures affect the effective diffusivity of Ag. In particular, $\langle D_{\mathrm{eff}} \rangle$ increases as temperature variation increases, which is expected due to the Arrhenius (exponential) dependence of $\langle D_{\mathrm{eff}} \rangle$ on temperature. Specifically, D_{eff} is larger in the case when the operating temperature is higher in the high-temperature regime (the region where time is larger than 300 days), in spite of the fact that the operating temperature is reduced by the same magnitude in the low-temperature regime (the region where time is smaller than 300 days). It shows that keeping the maximum temperature low is more important for reducing the overall Ag release than keeping the minimum temperature low. This data also shows that it is undesirable to have the temperature fluctuation that leads to temporary excursions to high temperatures because it may have a detrimental effect on Ag release. In order to confirm the effect of temperature variation on D_{eff}, we calculate D_{eff} when temperature decreases linearly as a function of time in 5 cases. The magnitude of temperature variation in these 5 cases is the same as that shown in Fig. 4a, and the only difference is that the temperature slope is negative such that the highest temperature occurs at the beginning instead of the end. We find that the results of $\langle D_{\mathrm{eff}} \rangle$ in these 5 cases are the same as that shown in Fig. 4b, which demonstrates that the direction (increase or decrease) of temperature change does not affect the dependence of $\langle D_{\mathrm{eff}} \rangle$ on temperature variation. In addition to the influence of temperature variation, we find that D_{eff} changes rapidly as f_{H} varies from 0.4 to 0.7 in all cases. This result indicates that D_{eff} is still strongly affected by the properties of GB networks even when temperature is time-dependent. Moreover, we also find that temperature variation does not dramatically affect the fluctuation and distribution of D_{eff} due to microstructural changes (see Figs. 5a and 5b). Therefore, based on Figs. 4 and 5 we conclude that, irrespectively of whether temperature is constant or time-dependent, the variation in GB structures can induce significant fluctuation in the effective diffusivity of Ag.

3.3. Effect of GB network properties on the Ag release fraction with time-dependent temperature and Ag generation rate

Up to this point we have focused on the dependence of the effective Ag diffusivity on GB structures. Another property of interest is the release fraction of Ag because it is directly related to the ability of SiC to retain Ag inside of fuel particles. As discussed in Section 2, when calculating the release fraction of Ag, we consider the generation rate of Ag to be time-dependent in order to be consistent with actual operating conditions. Figure 6a shows the normalized generation rate of Ag-110m as a function of time used in our simulations, which is obtained from the Ag inventory generation in one compact of the AGR-1 test [39]. The trend shown in Figure 6a (i.e., more Ag is generated at a later stage) is typically observed during irradiation due to several factors, including the higher yield of Ag-109 from plutonium fission [39]. We note that different Ag isotopes may have different generation rates. Here, we mainly focus on qualitative trends in Ag release resulting from a non-linear source generate rate and we do not investigate any quantitative effects of generation rate on Ag transport. We use temperature profiles shown in Fig. 4a to provide a meaningful comparison between our calculations of the effective diffusivities (reported in Sec. 3.2) and results of the release fraction of Ag studied here.

The release fraction is calculated by the methods described in Sec. 2. In simulations, we denote the diffusivity along virtual paths as D_{V}, where virtual paths connect a virtual node outside the SiC layer with nodes in the z- plane of the SiC TRISO layer (see Section 2). We then examine the dependence of Ag release fraction on the ratio $\frac{D_{\mathrm{V}}}{D_{\mathrm{H}}}$, where we vary D_{V} while keeping D_{H} constant. Figure 6b shows the Ag release fraction as a function of the ratio $\frac{D_{\mathrm{V}}}{D_{\mathrm{H}}}$ with different f_{H} in the Case 1 (shown in Fig. 4a). It is found that as $\frac{D_{\mathrm{V}}}{D_{\mathrm{H}}}$ increases, the Ag release fraction first increases, and then approaches a constant. The former (initial increase of Ag release fraction) is expected because higher D_{V} helps the Ag atom select a faster path to diffuse among the different GB paths. The latter (Ag release approaches a constant) indicates that the Ag release will saturate for large $\frac{D_{\mathrm{V}}}{D_{\mathrm{H}}}$. Since $\frac{D_{\mathrm{V}}}{D_{\mathrm{H}}}$ does not affect the Ag release fraction significantly when it is larger than 10, we set $\frac{D_{\mathrm{V}}}{D_{\mathrm{H}}} = 10$ in the following simulations. Figure 6c shows the release fraction of Ag at the 600^{th} day as a function of f_{H} with different temperature profiles. It is clear that with all temperature profiles the release fraction has a wide range of values when f_{H} changes from 0.4 to 0.7. Comparison of Figs. 6c and Fig. 4b shows that the dependence of the release fraction of Ag on f_{H} is consistent with the trend in the effective diffusivity, which is expected because the release of Ag is governed by its effective diffusivity in GB networks.

Figure 6 together with Figs. 2-5 shows that variation in properties of GB networks (including $\frac{D_{\mathrm{H}}}{D_{\mathrm{L}}}$, f_{H} and distribution of GBs) can induce fluctuation in the effective diffusivity and release fraction of Ag when temperature is either constant or time-dependent. It suggests that changes in GB structures in the SiC layer may have significant contributions to the scatter in the effective diffusivity and release fraction of Ag measured in experiments.

3.4. Effects of irradiation and temperature distribution on Ag diffusion

Calculations in Sections 3.1-3.3 demonstrate that the transport of Ag across the SiC layer is sensitive to the variation of GB structures when the diffusivities of Ag in HEGB and LEGB are consistent with the integral release experimental data. In order to further test the hypothesis that GB diffusion is the dominant transport mechanism of Ag in SiC, we now analyze kMC simulations

where the GB diffusivities were taken to match published quantitative data, instead of fitting the diffusivities to the release measurements. Through this analysis we can estimate if the release experiments can be quantitatively explained through GB diffusion alone. As discussed in Section 3, there is not enough data to map all the GB types onto Ag diffusivities, however there are a few experimental ion implantation studies [12, 21, 22, 35] and DFT simulations [25, 26] that provide reasonable bounds to consider in our simulations. The results from ion implantation experiments and DFT calculations, together with integral release experimental measurements [5–7, 40], are summarized in Fig. 7. In the same figure, we also show the effective diffusivity obtained by the present kMC model when LEGB and HEGB, respectively, are represented by $\Sigma 3$ GB and amorphous GB with diffusivities ($D_{\mathrm{L}} = 1.6 \times 10^{-7} \times \exp\left(\frac{-3.95}{kT}\right)$ m^2/s, and $D_{\mathrm{H}}^{\max} = 2.39 \times 10^{-10} \times \exp\left(\frac{-2.61}{kT}\right)$ m^2/s) obtained from Refs. [25] and [26]. Symbols in the figure correspond to experimental data and lines correspond to results from simulations. It can be seen that the diffusivities calculated in our model (red solid and red dotted lines) fall in the same range as the ones measured in ion-implantation experiments (black symbols). Interestingly, the diffusivity calculated in our model as well as those measured in ion-implantation experiments are visibly lower than those obtained from integral release experiments. The difference in the diffusivities between the calculated values and the integral release experimental data suggest that additional mechanisms or factors, which are not considered in the present model, may play an important role in Ag transport through SiC.

One potential factor is that Ag diffusion could be affected by radiation. Radiation effects have not been so far included in DFT calculations and ion-implantation experiments of Ag transport, but fuel particles are all irradiated during integral release experiments. Although the influence of a number of microstructural features on Ag transport are considered in Ref. [34], their effects are modeled by parametric functions where parameters are selected to fit experimental data, so the quantitative mechanism of the Ag transport under irradiation remains to be understood. A full investigation of radiation effects is beyond the scope of the current paper.

In addition to irradiation effects, another potential factor that could explain the difference between the diffusivities measured in reactor experiments and that measured in diffusion couple experiments (and predicted by DFT and our model) is the spatial and temporal fluctuations of temperature in reactors. It was shown in Ref. [9] that within a single AGR-1 capsule, the time average-volume average temperatures in compacts can differ by as much as 130°C, and within certain compacts, the temperature distribution may have a range of as much as 300°C (the difference between the minimum and the maximum temperature) due to the geometry of the irradiation capsule. It was also shown in Ref. [39] that the volume average temperature in compacts could vary over several hundred degrees Celsius over the course of the irradiation. The effect of temporal variation in temperature on the Ag diffusivity is demonstrated in Fig. 4b. It is expected that the spatial fluctuation of temperature may enhance the Ag diffusivity as well. In addition to increasing the magnitude of the Ag diffusivity, the temperature fluctuation in both space and time may also affect the spread the Ag diffusivity. We have shown in Fig. 7 that when the temperature changes by 300°C the effective diffusivity may vary by one or two orders of magnitude. Finally, it is also possible that fission products such as Pd may additionally accelerate Ag diffusion as discussed in Refs. [17–19].

There are other factors that may contribute to the scatter in Ag diffusivity observed in integral release experiments. The Ag diffusivity fluctuation shown in Fig. 3 corresponds to the contribution of GB distribution under constant temperature, f_{H} and $\frac{D_{\mathrm{H}}}{D_{\mathrm{L}}}$. In actual reactors, in addition to spatial and temporal temperature fluctuation mentioned above, f_{H} and $\frac{D_{\mathrm{H}}}{D_{\mathrm{L}}}$ may also vary amont

fuel particles. As shown in Fig. 2, variation in f_{H} and $\frac{D_{\mathrm{H}}}{D_{\mathrm{L}}}$ may change Ag diffusivity by more than one order of magnitude. Moreover, finite size of the sample may further contribute to the scatter in Ag diffusivity. By combining all these factors, the spread in the effective diffusivity is likely to be similar to that measured in integral release experiments.

4. Concluding remarks

We have developed a kinetic Monte Carlo model to evaluate the effective diffusivity and release fraction of Ag through polycrystalline SiC. It is found that the transport of Ag across the SiC layer is sensitive to the variation in GB network properties such as fraction of each GB type, spectrum in GB diffusivity and GB distributions. In particular, as properties of GB networks vary, the effective diffusivity and release fraction of Ag change significantly. Moreover, we find that the variation of the effective diffusivity and release fraction of Ag due to changes in GB structures is almost independent of temperature fluctuations. These results suggest that the variation in properties of GB networks in the SiC layer may contribute to the scatter in Ag diffusivity and release fraction measured in experiments.

Comparisons of laboratory experiments and modeling results with release from irradiated fuel particles strongly suggests that in actual fuel particles, diffusion of Ag is not only dependent on GB structures in SiC, but it is also affected by other factors such as irradiation and temperature distribution. In particular, various defect structures developed in SiC during irradiation may have a pronounced impact on Ag diffusion. Non-uniform temperature distribution may enhance the spread in the diffusivity and release fraction of Ag in individual fuel particles. Understanding the effects of irradiation and temperature distribution on Ag transport may help to resolve the discrepancy in the literature data on Ag diffusivities and is currently in progress.

Acknowledgment
This research is being performed using funding received from the DOE Office of Nuclear Energy's Nuclear Energy University Programs contract number 00089350.

References

[1] D. Olander, Nuclear fuels - present and future, J. Nucl. Mat., 389 (2009) 1-22.

[2] D. Petti, J. Buongiorno, J. Maki, R. Hobbins, G. Miller, Key difference in the fabrication, irradiation and high temperature accident testing of US and German TRISO-coated particle fuel, and their implications on fuel performance, Nucl. Eng. Des. 222 (2003) 281-297.

[3] N. van der Berg, J. Malherbe, A. Botha, E. Friedland, SEM analysis of the microstructure of the layers in triple-coated isotropic (TRISO) particles, Surf. Interface Anal. 42 (2010) 1156-1159.

[4] J. Malherbe, Diffusion of fission products and irradiation damage in SiC, J. Phys. D: Appl. Phys. 46 (2013) 473001.

[5] H. Nabielek, P. Brown, P. Offermann, Silver release from coated particle fuel, Nucl. Tech. 35 (1977) 483-493.

[6] W. Amian, D. Stover, Diffusion of silver and cesium in silicon-carbide coatings of fuel particles for high-temperature gas-cooled reactors, Nucl. Tech. 61 (1983) 475-486.

[7] K. Verfondern, R. Martin, R.Moormann, Methods and data for HTGR fuel performance and radionuclide release modeling during normal operation and accidents for safety analyese, Jul-2722 Forschungzentrum Julich GmbH, January (1993)

[8] R. Bullock, Fission-product release during post-irradiation annealing of several types of coated fuel particles, J. Nucl. Mat. 125 (1984) 304-319.

[9] P. Demkowicz, J. Hunn, R. Morris, J. Harp, P. Winston, C. Baldwin, F. Montgomery, Preliminary results of post-irradiation examination of the AGR-1 TRISO fuel compacts, HTR2012-3-027, Proceedings of the HTR 2012, Tokyo, Japan October 28-November 1 (2012)

[10] C. Baldwin, J. Hunn, R. Morris, F. Montgomery, C. Silva, P. Demkowicz, First elevated-temperature performance testing of coated particle fuel compacts from the AGR-1 irradiation experiment, Nucl. Eng. Des. 271 (2014) 131-141.

[11] Y. Katoh, L. Snead, I. Szlufarska, W. Weber, Radiation effects in SiC for nuclear structural applications, Current Opinion in Solid State and Materials Science, 16 (2012) 143-152.

[12] H. MacLean, R. Ballinger, L. Kolaya, S. Simonson, N. Lewis, M. Hanson, The effect of annealing at 1500C on migration and release of ion implanted silver in CVD silicon carbide, J. Nucl. Mat. 357 (2006) 31-47.

[13] H. MacLean, Silver transport in CVD silicon carbide, Ph.D. Thesis, MIT, Department of Nuclear Engineer, (2004)

[14] H. Xiao, Y. Zhang, L. Snead, V. Shutthanandan, H. Xue, W. Weber, Near-surface and bulk behavior of Ag in SiC, J. Nucl. Mat. 420 (2012) 123-130.

[15] K. Minato, K. Sawa, T. Koya, T. Tomita, A. Ishikawa, Fission product release behavior of individual coated fuel particles for high-temperature gas-cooled reactors, Nucl. Tech. 131 (2000) 36-47.

[16] E. Lopez-Honorato, H. Zhang, D. Yang, P. Xiao, Silver diffusion in Silicon Carbide coatings, J. Am. Ceram. Soc. 94 (2011) 3064-3071.

[17] E. Olivier, J. Neethling, Palladium transport in SiC, Nucl. Eng. Des. 244 (2012) 25-33.

[18] J. Neethling, J. O'Connell, E. Olivier, Palladium assisted silver transport in polycrystalline SiC, Nucl. Eng. Des. 251 (2012) 230-234.

[19] E. Olivier, J. Neethling, The role of Pd in the transport of Ag in SiC, J. Nucl. Mat. 432 (2013) 252-260.

[20] K. Minato, T.Ogawa, K. Fukuda, H. Sekino, H. Miyanishi, S. Kado, I. Takahashi, Release behavior of metallic fission products from HTGR fuel particles at 1600 to 1900C, J. Nucl. Mat. 202 (1993) 47-53.

[21] E. Friedland, J. Malherbe, N. van der Berg, T. Hlatshwayo, A. Botha, E. Wendler, W. Wesch, Study of silver diffusion in silicon carbide, J. Nucl. Mat. 389 (2009) 326-331.

[22] E. Friedland, N. van der Berg, J. Malherbe, J. Hancke, J. Barry, E. Wendler, W. Wesch, Investigation of silver and iodine transport through silicon carbide layers prepared for nuclear fuel element cladding, J. Nucl. Mat. 410 (2011) 24-31.

[23] E. Lopez-Honorato, D. Yang, J. Tan, P. Meadows, P. Xiao, Silver diffusion in coated fuel particles, J. Am. Ceram. Soc. 93 (2010) 3076-3079.

[24] T. Gerczak, B. Leng, K. Sridharan, J. Hunter Jr., A. Giordani, T. Allen, Observations of Ag diffusion in ion implanted SiC, to be published.

[25] S. Khalil, N. Swaminathan, D. Shrader, A. Heim, D. Morgan, I. Szlufarska, Diffusion of Ag along $\Sigma 3$ grain boundaries in 3C-SiC, Phys. Rev. B 84 (2011) 214104.

[26] H. Ko, J. Deng, I. Szlufarska, D. Morgan, Ag diffusion in SiC high energy grain boundaries: kinetic Monte Carlo study with first-principle calculations, in preparation.

[27] J. Rabone, E. Lopez-Honorato, P. van Uffelen, Silver and cesium diffusion dynamics at the β-SiC $\Sigma 5$ grain boundary investigated with density functional theory molecular dynamics and metadynamics, J. Phys. Chem. A 118 (2014) 915-926.

[28] D. Shrader, S. Khalil, T. Gerczak, T. Allen, A. Heim, I. Szlufarska, D. Morgan, Ag diffusion in cubic silicon carbide, J. Nucl. Mat. 408 (2011) 257-271.

[29] R. Kirchhofer, J. Hunn, P. Demkowicz, J. Cole, B. Gorman, Microstructure of TRISO coated particles from the AGR-1 experiment: SiC grain size and grain boundary character, J. Nucl. Mat. 432 (2013) 127-134.

[30] L. Tan, T. Allen, J. Hunn, J. Miller, EBSD for microstructure and property characterization of the SiC-coating in TRISO fuel particles, J. Nucl. Mat. 372 (2008) 400-404.

[31] D. Helary, O. Dugne, X. Bourrat, P. Jouneau, F. Cellier, EBSD investigation of SiC for HTR fuel particles, J. Nucl. Mat. 350 (2006) 332-335.

[32] J. Deng, D. Morgan, I. Szlufarska, Kinetic Monte Carlo simulation of the effective diffusivity in grain boundary networks, Comp. Mat. Sci., 93 (2014) 36-45.

[33] https://en.wikipedia.org/wiki/Voronoi_diagram.

[34] G. Meric de Bellefon, B. Wirth, Kinetic Monte Carlo (KMC) simulation of fission product silver transport through TRISO fuel particles, J. Nucl. Mat. 413 (2011) 122-131.

[35] T. Gerczak, Understanding Ag release from TRISO fuel through surrogate diffusion experiments and fuel analysis, Dissertation, University of Wisconsin - Madison, 2013.

[36] I. Kaur, Y. Mishin, W. Gust, Fundamentals of grain and interphase boundary diffusion, Wiley, Chichester, (1995)

[37] Y. Chen, C. Schuh, Diffusion on grain boundary networks: percolation theory and effective medium approximations, Acta Mater. 54 (2006) 4709-4720.

[38] B. Collin, AGR-1 irradiation test final as-run report, INL-EXT-10-18097 Revision 3, 2015.

[39] P. Demkowicz, B. Collin, AGR-1 silver release: comparison of experiment with PARFUME predictions, presentation in Very High Temperature Reactor Research and Development 2013 Technical Review Meeting, 2013.

[40] IAEA-TECDOC-978, Fuel performance and fission product behavior in gas cooled reactors, 1997.

Figure captions:

Figure 1: (Color online) Schematic view of the simulation domain. The SiC layer consists of 32×32 connected cubic cells, and each cell has the same Voronoi diagram but different grain boundary distributions. Virtual node and virtual paths are used when calculating the release fraction of Ag. See details in text.

Figure 2: (Color online) The effective diffusivity (a) as a function of the fraction of HEGBs with different diffusivity ratios and (b) as a function of the diffusivity ratio with different fractions of HEGBs.

Figure 3: (Color online) (a) Coefficient of variation of D_{eff} as a function of the HEGB fraction f_{H} for different diffusivity ratios $\frac{D_{\text{H}}}{D_{\text{L}}}$. (b) Distribution of D_{eff} with different f_{H} and $\frac{D_{\text{H}}}{D_{\text{L}}}$.

Figure 4: (Color online) (a) Temperature as a linear function of time with different slopes. In case 1, the temperature is a constant. (b) The effective diffusivity as a function of the fraction of HEGBs with different temperature profiles shown in (a).

Figure 5: (a) Coefficient of variation of D_{eff} as a function of the HEGB fraction f_{H} with different temperature profiles shown in Fig. 3a. (b) Distribution of D_{eff} with different temperature profiles and f_{H}.

Figure 6: (Color online) (a) Normalized Ag generation rate as a function of time. (b) The Ag release fraction as a function of $\frac{D_{\text{V}}}{D_{\text{H}}}$ with different f_{H} in the Case 1 shown in Figure 3a. (c) The Ag release fraction as a function of the f_{H} with different temperature profiles shown in Figure 3a.

Figure 7: Comparison of the Ag diffusivities measured in integral release experiments [5-7, 39], ion implantation experiments [12, 20, 21, 34] and DFT calculations [25, 26]. The blue dash-dot line and blue dash line are the diffusivities in $\Sigma 3$ GB [25] and the upper limit of the diffusivity in amorphous GB [26] obtained from DFT calculations without consideration of irradiation effect. The red dotted line and the red solid line are D_{eff} obtained from the present kMC model when f_{H} is 0.4 and 0.7, respectively, where LEGB and HEGB are represented by $\Sigma 3$ GB and amorphous GB, respectively.

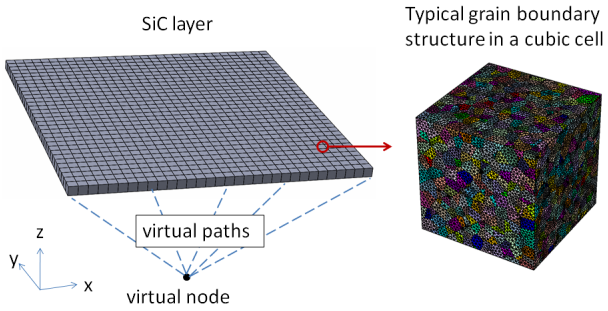

Figure 1: (Color online) Schematic view of the simulation domain. The SiC layer consists of 32×32 connected cubic cells, and each cell has the same Voronoi diagram but different grain boundary distributions. Virtual node and virtual paths are used when calculating the release fraction of Ag. See details in text.

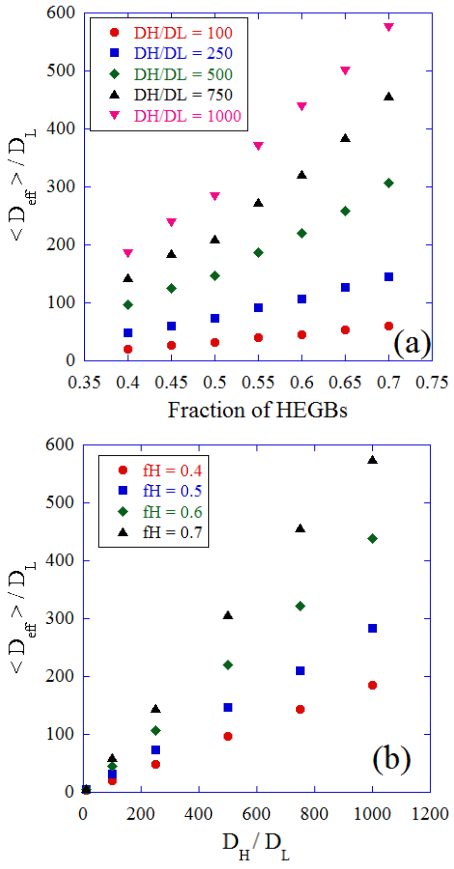

Figure 2: (Color online) The effective diffusivity (a) as a function of the fraction of HEGBs with different diffusivity ratios and (b) as a function of the diffusivity ratio with different fractions of HEGBs.

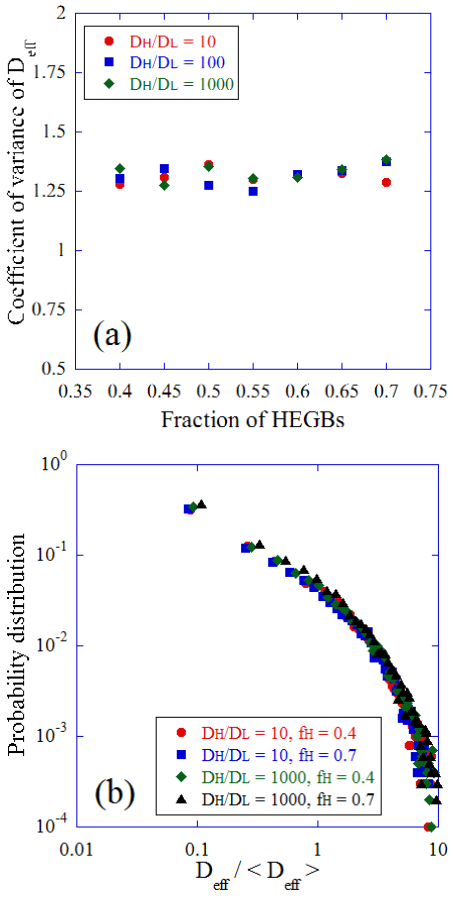

Figure 3: (Color online) (a) Coefficient of variation of D_{eff} as a function of the HEGB fraction f_{H} for different diffusivity ratios $\frac{D_{\text{H}}}{D_{\text{L}}}$. (b) Distribution of D_{eff} with different f_{H} and $\frac{D_{\text{H}}}{D_{\text{L}}}$.

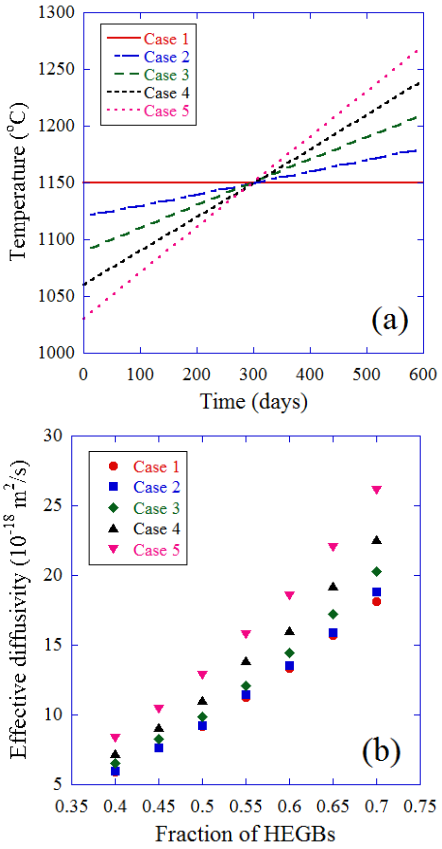

Figure 4: (Color online) (a) Temperature as a linear function of time with different slopes. In case 1, the temperature is a constant. (b) The effective diffusivity as a function of the fraction of HEGBs with different temperature profiles shown in (a).

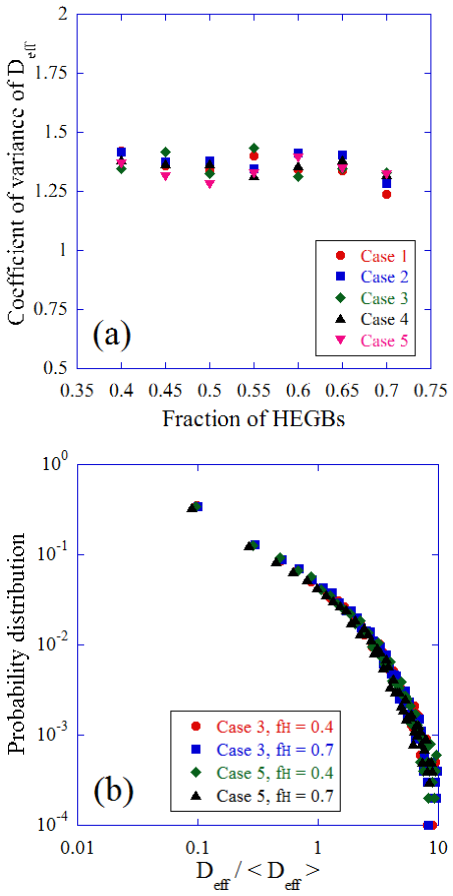

Figure 5: (Color online) (a) Coefficient of variation of $D_{\rm eff}$ as a function of the HEGB fraction $f_{\rm H}$ with different temperature profiles shown in Fig. 3a. (b) Distribution of $D_{\rm eff}$ with different temperature profiles and $f_{\rm H}$.

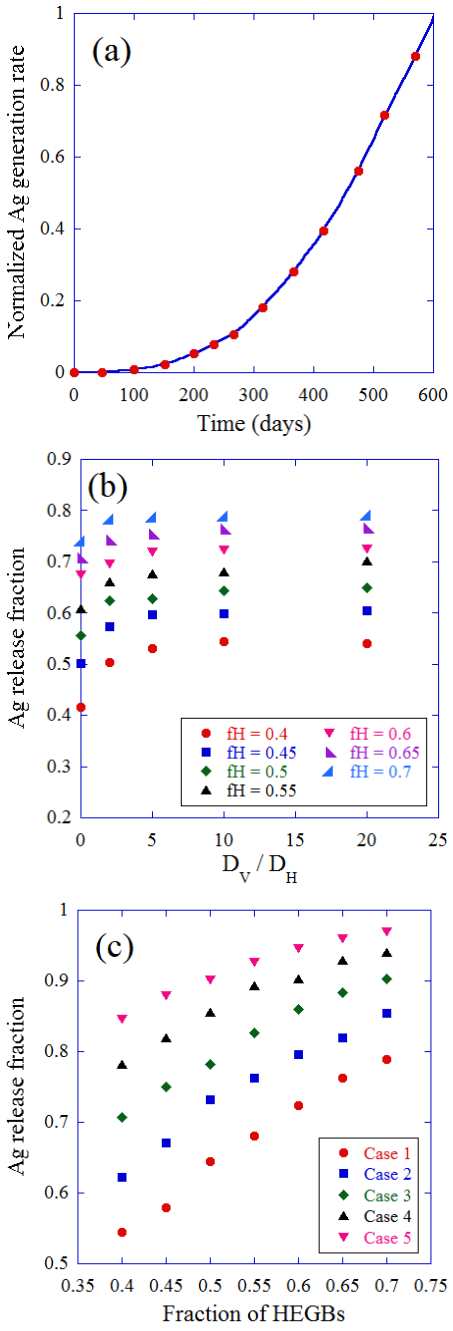

Figure 6: (Color online) (a) Normalized Ag generation rate as a function of time. (b) The Ag release fraction as a function of $\frac{D_V}{D_H}$ with different f_H in the Case 1 shown in Figure 3a. (c) The Ag release fraction as a function of the f_H with different temperature profiles shown in Figure 3a.

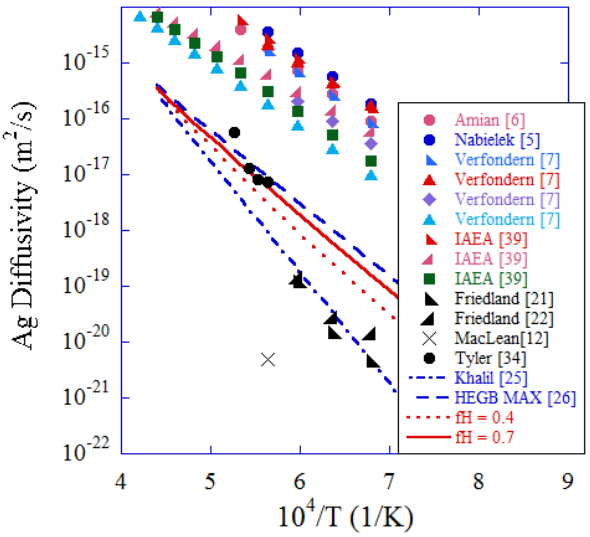

Figure 7: Comparison of the Ag diffusivities measured in integral release experiments [5-7, 39], ion implantation experiments [12, 20, 21, 34] and DFT calculations [25, 26]. The blue dash-dot line and blue dash line are the diffusivities in Σ3 GB [25] and the upper limit of the diffusivity in amorphous GB [26] obtained from DFT calculations without consideration of irradiation effect. The red dotted line and the red solid line are D_{eff} obtained from the present kMC model when f_{H} is 0.4 and 0.7, respectively, where LEGB and HEGB are represented by Σ3 GB and amorphous GB, respectively.